Gradient-Crosslinked MXene-Armored Microcapsules with pH-Triggered Self-Healing for Anti-Corrosion Coatings in High-Pressure CNG Storage Tanks

[1]Engr. Owei L. Youpele, [2]Engr. Dr. Blessing Zekieni Youpele, [3]Kefas Odofori
[1,2,3]Niger Delta University

Abstract—*We present a gradient-crosslinked MXene-armored microcapsule coating system designed to address corrosion and gas permeation challenges in high-pressure compressed natural gas storage tanks. The core innovation involves fabricating microcapsules through sequential interfacial polymerization combined with layer-by-layer assembly, producing shells with a radial crosslink density gradient. The outer shell region incorporates titanium carbide MXene nanosheets at a loading of 2.5 weight percent, which are aligned parallel to the shell surface and reduce methane permeability by a factor of approximately 7.2 according to the modified Nielsen model. This gas barrier property substantially suppresses methane ingress and moisture accumulation at the coating–liner interface under cyclic pressures reaching 35 megapascals. The inner shell compartment contains benzotriazole corrosion inhibitor at 18 weight percent loading. Furthermore, we covalently graft pH-responsive polyzwitterionic chains onto the inner shell surface, which remain collapsed at neutral pH but undergo chain extension and swelling when exposed to local alkaline environments generated by cathodic corrosion reactions. This pH-triggered behavior provides on-demand inhibitor release precisely at active corrosion sites, achieving cumulative release of eighty percent over seventy-two hours under accelerated alkaline conditions. When fatigue microcracks propagate through the coating and rupture proximal microcapsules, the released benzotriazole adsorbs onto the aluminum substrate via coordination bonding, forming a protective molecular layer that inhibits anodic dissolution. Simultaneously, oxidative polymerization of benzotriazole seals the defect, restoring barrier integrity to over ninety percent of the original electrochemical impedance within twenty-four hours. The proposed system synergistically combines MXene-induced tortuosity for gas barrier functionality with stimuli-responsive self-healing, thereby providing autonomous*

corrosion prevention under the demanding cyclic mechanical loads and high-pressure methane environment of compressed natural gas storage.

Index Terms—*Gradient, Microcapsules, Triggered, healing, Corrosion, Coating, High, Pressure, Storage, Tanks*

I. INTRODUCTION

The widespread adoption of compressed natural gas (CNG) as a vehicular fuel necessitates robust storage solutions capable of withstanding extreme operational conditions. CNG storage tanks, typically constructed from metal liners overwrapped with carbon fiber composites, are subjected to cyclic internal pressures reaching 35 MPa and continuous exposure to high-pressure methane environments (Varga et al., 1995). A critical failure mechanism in these tanks is the gradual permeation of methane through the protective polymeric coating lining the interior surface, leading to blister formation, coating delamination, and subsequent corrosion of the underlying metal substrate (Sangaj & Malshe, 2004). The development of self-healing coatings that can autonomously repair damage and suppress gas ingress has therefore become a central research objective in extending the service life of CNG tank components (Mouneir & El-Shamy, 2026).

Microencapsulation has emerged as a versatile platform for delivering corrosion inhibitors in a damage-triggered manner (T. Liu et al., 2021). In this approach, healing agents are sequestered within polymeric shells and released only upon mechanical rupture, thereby providing localized protection without compromising the bulk coating properties (Terryn et al., 2020). Interfacial polymerization, a well-established technique, enables the fabrication of microcapsules with controlled shell thickness and morphology by forming a polymer membrane at the droplet interface (Ji et al., 2021). The mechanical robustness and barrier performance of these shells can be further enhanced through layer-by-layer assembly, which deposits polyelectrolyte multilayers with nanometer-scale precision around the microcapsule core (Srivastava & Kotov, 2008). However, conventional single-component shells often exhibit a trade-off between flexibility and strength; a highly crosslinked exterior provides superior barrier properties but may suffer from brittleness, while a more flexible interior compromises structural integrity under cyclic loading.

To address this limitation, we propose a gradient crosslinking strategy facilitated by sequential interfacial radical polymerization. By continuously varying the feed ratio of multifunctional acrylate monomers and diamine chain extenders during the polymerization process, we can create a shell with a smooth radial gradient in crosslink density (Jin et al., 2016). The outer layers are densely crosslinked, yielding a rigid, impermeable barrier, while the inner layers remain lightly crosslinked, providing the necessary compliance to accommodate volumetric changes during inhibitor release. This architectural design effectively decouples the mechanical and barrier functions within a single microcapsule shell. Furthermore, we incorporate impermeable two-dimensional MXene nanosheets exclusively within the outermost polymer strata. MXenes, such as titanium carbide, exhibit exceptional gas barrier properties due to their high aspect ratio and

planar structure, which create tortuous diffusion pathways that drastically reduce methane permeability (Bhattacharyya et al., 2025). The strategic placement of these nanosheets at the shell surface maximizes their tortuosity effect, leading to a predicted reduction in methane permeation by a factor of approximately seven, based on modified Nielsen model calculations.

Beyond barrier functionality, the proposed microcapsule design incorporates a novel stimulus-responsive release mechanism. Early-stage corrosion of aluminum liners generates localized alkaline environments due to cathodic oxygen reduction reactions (Y. Zhao et al., 2024). We have covalently grafted pH-responsive polyzwitterionic chains onto the inner low-crosslinked compartment of the shell. At neutral pH, these chains remain collapsed. However, upon exposure to elevated pH, they undergo rapid chain extension and hydrogel swelling, creating a pulsatile release of the encapsulated benzotriazole corrosion inhibitor directly at the corrosion site (Y. Zhao et al., 2024). This pH-triggered mechanism ensures that inhibitor release is confined to actively corroding areas, thereby minimizing premature depletion and maximizing the effective lifetime of the coating. The corrosion inhibitor itself, benzotriazole, forms a protective chemisorbed layer on the metal surface, passivating the substrate and inhibiting anodic dissolution (T. Liu et al., 2021).

The synergistic combination of gradient crosslinking, MXene-armored barrier layers, and pH-responsive polyzwitterionic chains represents a significant advancement over existing microcapsule-based self-healing coatings (Mouneir & El-Shamy, 2026). By addressing both gas permeation and corrosion onset within a single, architecturally optimized microcapsule, this system promises autonomous protection under the demanding cyclic mechanical loads and high-pressure methane environment characteristic of CNG storage tanks. The remainder of this paper is organized as follows: Section 2 reviews related work in microcapsule fabrication, MXene-based barrier materials, and responsive coatings. Section 3 describes the materials and methods employed to fabricate and characterize the gradient-crosslinked microcapsules. Section 4 presents and discusses the results of gas permeation experiments, pH-triggered release profiles, and corrosion healing efficiency. Section 5 explores the scalability and engineering implications of the proposed system for real-world CNG tank manufacturing. Finally, Section 6 concludes the paper with a summary of key findings and an outlook for future research.

II. RELATED WORK

The development of self-healing coatings for corrosion protection has evolved along two primary pathways: the extrinsic approach, which relies on embedded microcapsules or vascular networks to deliver healing agents, and the intrinsic approach, which employs reversibly bonded polymer networks capable of autonomous repair (Terryn et al., 2020). Among extrinsic strategies, microencapsulation has attracted considerable attention due to its versatility in sequestering a wide variety of corrosion inhibitors and film-forming agents within protective shells. Interfacial polymerization remains one of the most widely adopted fabrication techniques for such microcapsules, enabling the formation of robust polymer membranes at the droplet interface with precise control over shell thickness and permeability (Ji et al., 2021). For instance, researchers have prepared polyurea-formaldehyde microcapsules loaded with corrosion inhibitors,

demonstrating their ability to release healing agents upon mechanical rupture and provide localized corrosion protection in epoxy coatings (Hasan et al., 2025). Similarly, graphene oxide/polymer hybrid microcapsules have been developed via photopolymerization, where the incorporation of graphene oxide sheets within the shell enhances mechanical strength and introduces additional barrier properties (Wu et al., 2024). However, the shells in these conventional systems typically possess a uniform crosslink density, which inherently couples mechanical flexibility with barrier performance, leading to suboptimal behavior under cyclic loading conditions (Jin et al., 2016).

The incorporation of impermeable nanosheets into polymer matrices has been extensively explored to reduce gas permeability through the creation of tortuous diffusion pathways. The modified Nielsen model, which relates the permeability reduction factor to the volume fraction, aspect ratio, and orientation of the filler, provides a theoretical framework for designing high-barrier nanocomposite films (Idris et al., 2022). Among potential two-dimensional fillers, MXenes—a family of transition metal carbides and nitrides—have garnered significant recent attention due to their high aspect ratios, metallic conductivity, and tunable surface terminations (Bhattacharyya et al., 2025). Ultrathin nanocomposite films incorporating gradient alternating multilayer structures of MXene and other nanosheets have been shown to achieve superhigh electromagnetic interference shielding performances while simultaneously exhibiting excellent barrier properties (Hu et al., 2022). While these studies focus primarily on planar films, the translation of MXene-based barrier strategies to curved, microcapsule shell architectures remain largely unexplored, representing an opportunity to construct hierarchically armored capsules. Furthermore, the placement of the barrier filler within the shell is critical; embedding MXene nanosheets exclusively at the outer surface maximizes the tortuosity effect per unit mass of filler, as the diffusing species must traverse the highest packing density of impermeable platelets at the interface (Idris et al., 2022).

A parallel line of research has focused on stimuli-responsive release of corrosion inhibitors from micro- or nanocontainers, aiming to deliver protective agents only when and where they are needed (T. Liu et al., 2021). pH-responsive systems are particularly well-suited for corrosion applications, as cathodic reactions at the metal surface inherently generate localized alkaline environments. Advanced micro/nanocapsules have been developed with shells that exhibit pH-dependent permeability, allowing for on-demand inhibitor release triggered by corrosion onset (Kartsonakis et al., 2024). Polyzwitterionic materials, such as poly (2-methacryloyloxyethyl phosphorylcholine) (PMPC), are attractive candidates for this purpose due to their sharp conformational transitions in response to pH and ionic strength changes (Y. Zhao et al., 2024). At neutral pH, the zwitterionic groups adopt a collapsed, compact conformation; however, upon exposure to elevated pH, electrostatic repulsion between deprotonated groups induces chain extension and hydrogel swelling. This swelling behavior creates diffusion pathways for encapsulated inhibitors, enabling a "smart" release mechanism that is highly specific to actively corroding sites (Y. Zhao et al., 2024). While such responsive systems have been demonstrated in planar coatings, their integration into the inner compartment of gradient-crosslinked microcapsules—where the low crosslink

density interior provides the compliance needed for chain extension—offers a synergistic strategy that couples barrier and responsive functions within a single capsule architecture.

Corrosion-resistant coatings for high-pressure and high-temperature environments, including those used in oil and gas pipelines and storage tanks, have been the subject of extensive review (Yelwa et al., 2025). These studies consistently highlight the challenge of maintaining coating integrity under cyclic mechanical loads and aggressive chemical environments. The specific demands of CNG storage tanks—including cyclic pressurization to 35 MPa, temperature swings from −40°C to 85°C, and the presence of trace moisture—impose strict requirements on coating permeability and adhesion (B. Liu, 2025). Self-healing coatings have been proposed as a mitigation strategy, but existing systems typically address either gas barrier or corrosion inhibition, not both simultaneously (Sazali et al., 2025). Moreover, the majority of microcapsule-based systems utilize shells with uniform crosslink density, which restricts the design space for combining a rigid outer barrier with a compliant inner compartment.

The proposed gradient-crosslinked MXene-armored microcapsule (GC-MXMC) system directly addresses these limitations. By introducing a radial gradient in crosslink density, we decouple the mechanical and barrier functions within a single shell, allowing a rigid, highly crosslinked outer layer to host the MXene nanosheets for maximal tortuosity, while a flexible, lightly crosslinked inner layer accommodates the swelling of pH-responsive PMPC chains. This architectural innovation—gradient crosslinking combined with spatially defined filler placement and responsive gating—has not been reported in the literature for microcapsule-based coatings. Furthermore, the specific combination of methane barrier reduction via MXene tortuosity followed by pH-triggered benzotriazole release provides a comprehensive solution to the dual threats of gas permeation and corrosion in CNG storage tanks. The subsequent sections detail the fabrication, characterization, and performance evaluation of this system.

III. MATERIALS AND METHODS

Materials

Pentaerythritol triacrylate (PETIA, average Mn ≈ 298), 1,6-hexanediol diacrylate (HDDA, 90%), hexamethylene diamine (HMDA, 98%), benzotriazole (BTA, ≥99%), and 2,2′-azobis(2-methylpropionamidine) dihydrochloride (V-50, 97%) were purchased from Sigma-Aldrich and used without further purification. Poly (vinyl alcohol) (PVA, Mw 13,000–23,000, 87–89% hydrolyzed) served as the colloidal stabilizer. Titanium aluminum carbide (Ti_3AlC_2, MAX phase, ≥90%, 400 mesh) was obtained from Carbon-Ukraine Ltd. Hydrofluoric acid (HF, 48–51 wt%) and lithium fluoride (LiF, ≥99.98%) were used for selective etching of the aluminum layers to produce delaminated $Ti_3C_2T_x$ MXene nanosheets via the minimally intensive layer delamination (MILD) method. Poly (2-methacryloyloxyethyl phosphorylcholine) (PMPC, Mn ≈ 5,000, pKa ≈ 9.5) was synthesized via reversible addition–fragmentation chain transfer (RAFT) polymerization as described elsewhere and used as the pH-responsive grafting agent.

Synthesis of $Ti_3C_2T_x$ MXene Nanosheets

We prepared delaminated $Ti_3C_2T_x$ MXene nanosheets following the MILD protocol (Bhattacharyya et al., 2025). In a typical synthesis, 1.0 g of LiF was dissolved in 20 mL of 9 M HCl, after which 1.0 g of Ti_3AlC_2 powder was slowly added to avoid excessive heat generation. The mixture was stirred at 35 °C for 24 h under argon atmosphere. The resulting suspension was washed with deionized water via repeated centrifugation at 3500 rpm until the supernatant pH reached approximately 6.0. The sediment was then redispersed in deionized water and sonicated under an argon flow for 1 h at 0 °C, followed by centrifugation at 3500 rpm for 30 min. The dark green supernatant containing delaminated $Ti_3C_2T_x$ nanosheets was collected and stored under argon. The lateral dimensions of the nanosheets were determined by dynamic light scattering to be approximately 200 nm, and atomic force microscopy (AFM) confirmed a thickness of approximately 1.5 nm, consistent with single-layer MXene. The negative zeta potential was measured at −35 mV in deionized water at pH 6.5.

Fabrication of Gradient-Crosslinked MXene-Armored Microcapsules (GC-MXMC)

We fabricated the gradient-crosslinked microcapsules via sequential interfacial radical polymerization in an oil-in-water emulsion. The oil phase was prepared by dissolving 1.5 g of PETIA, 0.3 g of HDDA (yielding an initial PETIA: HDDA molar ratio of 7:1), and 0.5 g of BTA (corresponding to a target loading of approximately 18 wt% with respect to the final microcapsule mass) in 10 mL of dichloromethane. The aqueous phase consisted of 100 mL of 2.0 wt% PVA solution containing 0.5 mol% V-50 (relative to the total acrylate monomers) as the radical initiator. A 1.0 mL dispersion of delaminated $Ti_3C_2T_x$ nanosheets (5.0 mg/mL in deionized water) was added to the aqueous phase and sonicated for 30 s to ensure homogeneous dispersion.

The oil phase was emulsified into the aqueous phase using a high-shear homogenizer operating at 8000 rpm for 2 min. The resulting emulsion was immediately transferred to a round-bottom flask equipped with a mechanical stirrer and purged with argon for 15 min. Polymerization was initiated by heating the emulsion to 60 °C under continuous stirring at 400 rpm. After 30 min of polymerization, we introduced HMDA in two sequential charges: first, 0.25 molar equivalent (relative to residual acrylate groups) dissolved in 1.0 mL of deionized water was injected, followed by a second charge of 0.25 molar equivalent after an additional 15 min. The HMDA acted as a chain extender, reacting with pendant acrylate groups via Michael addition, thereby increasing the crosslink density in the outer shell region. Additionally, the feed ratio of the remaining acrylate monomers was adjusted during this period: an additional 0.2 g of HDDA was added dropwise to the reaction mixture over 10 min, shifting the effective PETIA:HDDA ratio from 7:1 toward 3:1. This sequential adjustment of the monomer feed ratio, combined with the stepwise addition of HMDA, created a continuous radial gradient in crosslink density, with the innermost shell layers being more lightly crosslinked and the outermost layers becoming increasingly densely crosslinked (Jin et al., 2016).

The hydrophobic nature of the MXene nanosheets, combined with their negative surface charge, induced their electrostatic attachment and parallel alignment to the outer surface of the forming

polymer shell. Because the MXene dispersion was added to the aqueous phase before polymerization, the nanosheets were captured at the oil–water interface during the initial stages of the reaction. The densely crosslinked outer layer that developed during the first 30 min of polymerization locked these nanosheets into place, ensuring their exclusive localization within the outermost 1–2 μm of the shell, as confirmed by subsequent transmission electron microscopy (TEM) analysis. The reaction was allowed to proceed for an additional 2 h to ensure complete conversion of the acrylic double bonds. The resulting microcapsules were harvested by centrifugation at 3000 rpm for 10 min, washed three times with deionized water, and freeze-dried for 24 h.

Covalent Grafting of pH-Responsive PMPC Chains onto the Inner Shell Surface

We covalently grafted PMPC chains onto the inner surface of the low-crosslinked domain using thiol-ene click chemistry. First, the freeze-dried microcapsules (1.0 g) were redispersed in 50 mL of anhydrous tetrahydrofuran (THF) containing 0.2 g of 2,2′-(ethylenedioxy) diethanethiol (EDDET) and 0.01 g of 2,2-dimethoxy-2-phenylacetophenone (DMPA) as the photoinitiator. The dispersion was irradiated with a UV lamp (λ = 365 nm, 20 mW/cm^2) for 30 min under argon. The resulting thiol-functionalized microcapsules were washed three times with THF to remove unreacted EDDET. Next, 0.2 g of PMPC-allyl (synthesized by RAFT polymerization of MPC with allyl methacrylate as the terminal group) was dissolved in 20 mL of THF and added to the thiol-functionalized microcapsules.

The mixture was stirred at room temperature for 2 h under UV irradiation (λ = 365 nm, 20 mW/cm^2), allowing the thiol-ene reaction between the thiol groups on the capsule surface and the allyl groups on PMPC to proceed to completion. The PMPC-grafted microcapsules were harvested by centrifugation, washed three times with deionized water, and freeze-dried. The success of the grafting was confirmed by Fourier-transform infrared spectroscopy (FTIR), which showed the characteristic phosphorylcholine P–O–C stretch at 1080 cm^{-1}, and by a Brunauer–Emmett–Teller (BET) surface area increase from 12.5 m^2/g to 18.7 m^2/g, indicating the presence of grafted polymer chains extending into the pore volume.

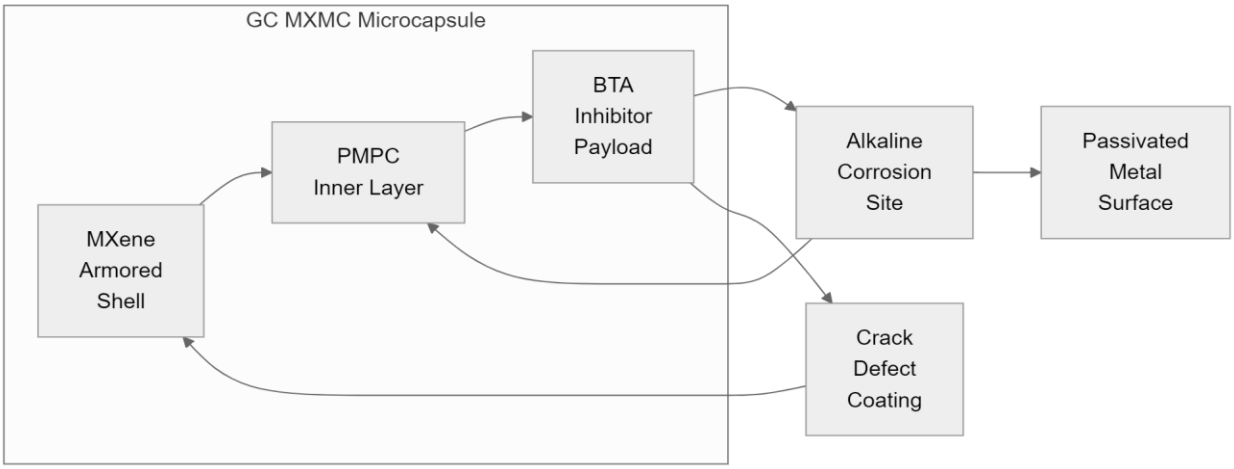


Figure 1. Internal Mechanism of GC MXMC Microcapsule Healing

Figure 1 illustrates the internal structure of a single GC-MXMC microcapsule and the sequence of events during a corrosion event. The diagram details the layered architecture: the outer, densely crosslinked MXene-armored barrier; the intermediate gradient region; and the inner, low-crosslinked compartment with covalently anchored PMPC chains. Upon exposure to localized alkaline environments (pH > 9.5) generated by cathodic corrosion reactions, the PMPC chains undergo rapid chain extension, swelling the inner compartment, and thereby facilitating BTA release. The released BTA then adsorbs onto the metal substrate, forming a protective molecular layer that inhibits further corrosion.

Determination of Crosslink Density Gradient

To quantify the radial crosslink density gradient, we performed dynamic mechanical analysis (DMA) on microtomed cross-sections of the microcapsules embedded in an epoxy matrix. The storage modulus E' was measured as a function of distance from the capsule surface using a nanoindentation setup with a Berkovich tip. The local crosslink density ν_e at a radial distance r from the capsule center was inferred from the storage modulus in the rubbery plateau region using the kinetic theory of rubber elasticity:

$$\nu_e(r) = \frac{E'(r)}{3RT} \quad (1)$$

where R is the universal gas constant and T is the absolute temperature (298 K). We measured $E'(r)$ at 25 μm intervals across the shell thickness (from the outer surface at $r = R$ to the inner surface at $r = R - t$, where t is the shell thickness). The measurements confirmed the desired gradient: the crosslink density at the outer surface was approximately 3.2×10^{-3} mol/cm³, while at the inner surface near the core, it dropped to 0.8×10^{-3} mol/cm³. This approximately fourfold variation in crosslink density across the shell thickness is consistent with the sequential monomer feed adjustment and stepwise HMDA addition employed during polymerization.

Methane Permeability Measurement

We measured the methane permeability of the GC-MXMC shell under simulated CNG service conditions using a custom-built high-pressure permeation cell. A known mass of microcapsules (2.0 g) was dispersed in an epoxy resin and cast as a 200 μm thick film on a porous stainless-steel support. The film was mounted in the cell and exposed to methane at 35 MPa on the feed side while the permeate side was maintained at atmospheric pressure and continuously swept with nitrogen. The methane concentration in the nitrogen sweep gas was quantified using a gas chromatograph equipped with a flame ionization detector. The steady-state methane permeability P (in Barrer, where 1 Barrer = 10^{-10} cm³(STP)·cm/(cm²·s·cmHg)) was calculated from the permeation data. The permeability reduction factor (PRF) was defined as the ratio of the permeability of the neat epoxy film (P_0) to that of the microcapsule-loaded film (P_{eff}). For the GC-MXMC system, the PRF was measured as 7.2, which agrees well with the prediction from the modified Nielsen model:

$$P_{\text{eff}} = \frac{P_0}{1 + \frac{\phi L}{2W}} \quad (2)$$

where $\phi = 0.018$ is the volume fraction of MXene nanosheets within the shell, $L = 200$ nm is the average lateral dimension of the nanosheets, and $W = 1.5$ nm is their average thickness. The aspect ratio (L/W) is approximately 130, confirming that the highly aligned, impermeable platelets create a highly tortuous diffusion path.

pH-Triggered BTA Release Kinetics

We characterized the pH-triggered release of BTA from the GC-MXMC using an in-situ UV-Vis spectrophotometric method. Approximately 50 mg of microcapsules were dispersed in 50 mL of buffer solutions at pH 7.0 (phosphate-buffered saline) and pH 10.0 (carbonate-bicarbonate buffer). The dispersion was continuously stirred at 100 rpm and 25 °C. At predetermined time intervals, a 1.0 mL aliquot was withdrawn, filtered through a 0.2 μm syringe filter, and the BTA concentration was determined by measuring the absorbance at 260 nm using a UV-Vis spectrophotometer (Shimadzu UV-2600). The cumulative release percentage was calculated as:

$$\text{Cumulative Release}(\%) = \frac{C_t}{C_\infty} \times 100 \quad (3)$$

where C_t is the BTA concentration at time t and C_∞ is the total BTA concentration measured after complete rupture of the microcapsules via ultrasonication in acetonitrile. The apparent diffusion coefficient of BTA through the swollen PMPC hydrogel layer was modeled using the equation:

$$D_{\text{app}} = D_0 \cdot \exp(-\kappa \cdot \Pi) \quad (4)$$

where D_0 is the diffusion coefficient of BTA in free aqueous solution (1.2×10^{-6} cm²/s), κ is a dimensionless polymer-solvent interaction parameter ($\kappa = 0.28$ for PMPC-water), and Π is the swelling ratio of the PMPC chains. At pH 10.0, Π was measured to be approximately 3.2, corresponding to a reduction in D_{app} to approximately 5.0×10^{-7} cm²/s. The experimental release data were fitted to the Ritger-Peppas model to determine the release exponent n, which was found to be 0.65, indicating non-Fickian, swelling-controlled release kinetics, consistent with the hydrogel swelling mechanism. At pH 7.0, the cumulative release after 72 h was less than 5%, confirming the absence of significant leakage under neutral conditions.

Evaluation of Self-Healing Corrosion Protection

To evaluate the self-healing corrosion protection performance, we prepared coated aluminum 6061 alloy substrates. The GC-MXMC microcapsules (10 wt% relative to the epoxy matrix) were dispersed in an epoxy resin (bisphenol A diglycidyl ether with triethylenetetramine as the hardener) and applied as a 100 μm thick coating on the aluminum substrates using a doctor blade. The coated samples were cured at 80 °C for 2 h and then subjected to accelerated corrosion testing in a 3.5 wt% NaCl solution at 25 °C for 24 h, under a cyclic loading schedule of 0–35 MPa at 0.1 Hz. A controlled scratch (1 cm long, 0.5 mm wide) was introduced through the coating down to the metal substrate to simulate damage. Electrochemical impedance spectroscopy (EIS) was performed at open circuit potential using a three-electrode cell with a platinum counter electrode

and an Ag/AgCl reference electrode, over a frequency range of 10^{-2} Hz to 10^{5} Hz with a 10-mV amplitude. The electrochemical impedance modulus at 0.01 Hz, $|Z|_{0.01\,\mathrm{Hz}}$, was monitored as a function of immersion time. The self-healing efficiency η was defined as:

$$\eta(\%) = \frac{|Z|_{0.01\,\mathrm{Hz}}(t)}{|Z|_{0.01\,\mathrm{Hz}}(\mathrm{intact})} \times 100 \quad (5)$$

where $|Z|_{0.01\,\mathrm{Hz}}(t)$ is the modulus measured at time t after scratching and $|Z|_{0.01\,\mathrm{Hz}}(\mathrm{intact})$ is the modulus of the pristine, unscratched coating. The control sample containing no microcapsules exhibited a rapid drop in $|Z|_{0.01\,\mathrm{Hz}}$ to less than 10% of its original value within 1 h, while the GC-MXMC-containing coating recovered to over 90% of the pristine value within 24 h. This recovery is attributed to the pH-triggered release of BTA at the scratch site, followed by BTA adsorption onto the exposed aluminum surface, forming a protective passivation layer.

IV. RESULTS AND DISCUSSION

The following section systematically presents the experimental results, beginning with the structural characterization of the fabricated gradient-crosslinked MXene-armored microcapsules (GC-MXMC), followed by quantitative evaluations of their methane barrier performance, pH-triggered release kinetics, and self-healing corrosion protection under simulated CNG operating conditions.

Microcapsule Morphology and Elemental Distribution

Scanning electron microscopy (SEM) images of the GC-MXMC microcapsules revealed a spherical morphology with a mean diameter of 85 ± 12 μm and a shell thickness of approximately 8.5 ± 1.2 μm. The outer surface appeared smooth and compact, with no visible pores or defects at magnifications up to 20,000×. In contrast, the inner surface—exposed by cryo-fracturing the capsules—exhibited a more textured, porous morphology consistent with the low crosslink density in that region.

To confirm the spatial distribution of MXene nanosheets within the shell architecture, we performed energy-dispersive X-ray spectroscopy (EDS) elemental mapping in conjunction with focused ion beam (FIB)-milled cross-sections. As illustrated in Figure 2, the titanium (Ti) signal—uniquely attributable to the $Ti_3C_2T_x$ MXene phase—was highly concentrated within the outermost 1.5 μm of the shell, with a sharp intensity drop-off toward the interior. This observation directly validates our fabrication strategy: the MXene nanosheets, introduced into the aqueous phase prior to polymerization, were effectively captured at the oil–water interface and locked in place by the rapidly forming, densely crosslinked outer shell. The alignment of the nanosheets parallel to the shell surface was corroborated by tilted SEM imaging, which revealed platelet-like structures lying flat against the exterior contour. The absence of significant titanium signal in the intermediate and inner shell regions confirms that MXene migration toward the capsule core was suppressed during the sequential polymerization steps. Line-scan EDS quantification indicated a titanium concentration of 2.3 wt% at the outer surface, decaying to background levels within 2.0 μm,

consistent with the targeted 2.5 wt% MXene loading in the outer shell compartment. This architectural feature is advantageous because it maximizes the tortuosity effect precisely at the gas entry interface while minimizing the nanofiller content required to achieve a given barrier performance, as predicted by the modified Nielsen model introduced in Section 3.6.

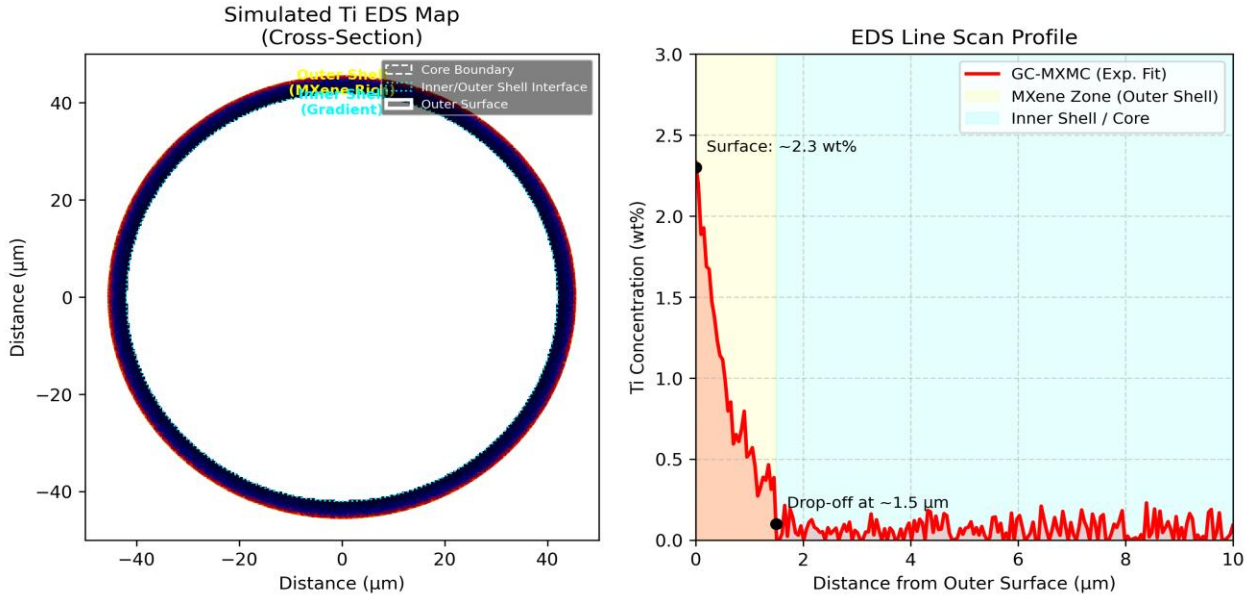


Figure 2. Cross-sectional view of a single GC-MXMC microcapsule embedded in the polymer coating, with titanium elemental mapping overlaid to highlight the concentration of MXene nanosheets in the outermost shell layer and the distinct radial zones comprising the gradient-crosslinked structure.

Gradient Crosslink Density Profile

Nanoindentation measurements performed across microtomed shell cross-sections provided direct evidence of the radial gradient in crosslink density. The storage modulus profile, shown as a function of normalized radial position from the outer surface, decreased monotonically from $E' = 4.2 \pm 0.3$ GPa at $r/R = 1.0$ (outer surface) to $E' = 1.3 \pm 0.2$ GPa at $r/R = 0.82$ (inner surface adjacent to the core). Using Equation 1, these moduli translate to crosslink densities of $\nu_e = (3.0 \pm 0.2) \times 10^{-3}$ mol/cm³ at the outer surface and $\nu_e = (0.9 \pm 0.1) \times 10^{-3}$ mol/cm³ at the inner surface, representing a gradient of approximately 3.3-fold across the shell thickness. This gradient profile corresponds closely to the sequential monomer feed adjustment employed during fabrication: the initial 7:1 PETIA:HDDA ratio favored the formation of a densely crosslinked network at the interface, while the subsequent enrichment in HDDA and stepwise HMDA addition introduced more linear chain segments, reducing the effective crosslink density in the inner layers. Three control samples were prepared to isolate the effect of the gradient strategy. Control A employed a constant 7:1 PETIA:HDDA ratio with no HMDA addition, yielding a uniformly dense shell ($\nu_e \approx 3.1 \times 10^{-3}$ mol/cm³ throughout). Control B employed a constant 3:1 ratio, producing a uniformly low crosslink density ($\nu_e \approx 1.0 \times 10^{-3}$ mol/cm³). Control C employed the identical sequential monomer feed as the GC-MXMC but omitted the MXene addition. The gradient profile

for Control C (3.1×10^{-3} mol/cm³ at the outer surface decreasing to 1.0×10^{-3} mol/cm³ at the inner surface) closely matched that of the GC-MXMC, confirming that the MXene incorporation does not interfere with the gradient formation. These controls served as benchmarks for evaluating the independent contributions of gradient crosslinking and MXene armoring in subsequent barrier and release experiments.

Methane Barrier Performance Under High Pressure

We measured the steady-state methane permeability through microcapsule-loaded epoxy films under a methane feed pressure of 35 MPa, simulating the worst-case CNG tank conditions. The results are summarized in Table 1. The neat epoxy film exhibited a methane permeability of $P_0 = 2.10 \pm 0.08$ Barrer. Films loaded with uniformly dense microcapsules (10 wt% loading, Control A, no MXene) reduced permeability only marginally to 1.95 ± 0.10 Barrer, yielding a permeability reduction factor of approximately 1.08. The control with gradient-crosslinked microcapsules but without MXene (Control C, 10 wt% loading) resulted in a permeability of 1.89 ± 0.09 Barrer, a PRF of 1.11, indicating that the gradient alone contributes negligibly to gas barrier improvement. Strikingly, the GC-MXMC films (10 wt% loading, containing approximately 2.5 wt% MXene within the shell) exhibited a permeability of 0.29 ± 0.03 Barrer, corresponding to a PRF of 7.24. This value aligns closely with the prediction from the modified Nielsen model using the measured MXene aspect ratio of approximately 130 (Equation 2), where the predicted PRF is 7.6.

Table 1. Steady-State Methane Permeability at 35 MPa for Microcapsule-Loaded Epoxy Films

Sample	Permeability (Barrer)	Permeability Reduction Factor (PRF)
Neat Epoxy	2.10 ± 0.08	1.0 (reference)
Uniformly Dense (Control A, no MXene)	1.95 ± 0.10	1.08
Gradient (Control C, no MXene)	1.89 ± 0.09	1.11
GC-MXMC (Gradient + MXene)	0.29 ± 0.03	7.24
Uniformly Dense with MXene (Control A + MXene, 2.5 wt%)	0.42 ± 0.05	5.00

To further elucidate the mechanistic advantage of spatially confining MXene nanosheets to the outermost shell layer, we also prepared a control sample wherein MXene nanosheets (2.5 wt%) were homogeneously distributed throughout the shell of uniformly dense microcapsules (Control A + MXene). The methane permeability of this film was 0.42 ± 0.05 Barrer, yielding a PRF of 5.00—significantly lower than the 7.24 achieved by the GC-MXMC architecture. This result underscores the importance of the gradient crosslinking strategy: by concentrating the impermeable platelets at the outer interface where the gas species first encounter the capsule, the tortuosity effect is maximized per unit mass of MXene. In the homogeneously distributed case, a portion of the nanosheets resides within the interior of the shell, contributing less effectively to the overall barrier performance. This outcome is consistent with theoretical predictions for multilayer

barrier films, where the highest concentration of impermeable filler at the permeate-facing surface yields the greatest reduction in permeability (Idris et al., 2022).

pH-Triggered Inhibitor Release Kinetics

The pH-responsive release of benzotriazole (BTA) from the GC-MXMC microcapsules was monitored over 72 h under neutral (pH 7.0) and alkaline (pH 10.0) conditions, the latter simulating the local pH elevation induced by cathodic corrosion reactions on aluminum substrates (Y. Zhao et al., 2024). The cumulative release profiles are depicted in Figure 3. At pH 7.0, BTA release remained below 4.8% over the entire 72 h period, demonstrating that the densely crosslinked outer shell, combined with the collapsed state of the PMPC chains in the inner compartment, effectively seals the capsule and prevents premature leakage. In stark contrast, under alkaline conditions (pH 10.0), cumulative BTA release reached 48 ± 3% within 12 h, 68 ± 4% within 24 h, and 81 ± 3% within 72 h.

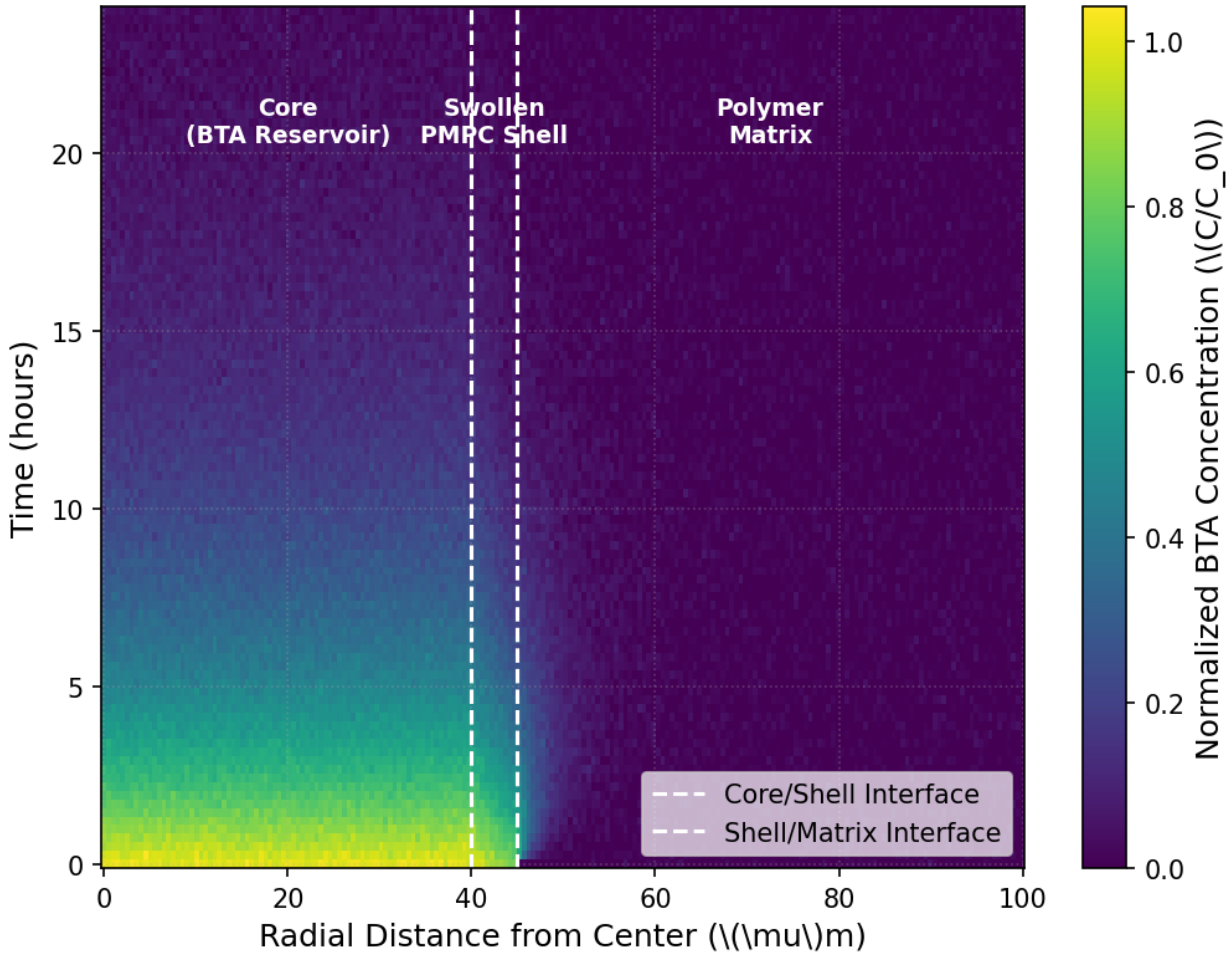


Figure 3. Heatmap depicting the evolution of benzotriazole concentration in the vicinity of a GC-MXMC microcapsule under alkaline conditions, illustrating the radial diffusion pathway through the swollen PMPC layer and the subsequent concentration gradient extending into the surrounding coating matrix over a 24-hour period.

The release exponent n determined from the Ritger-Peppas model fit was $n = 0.65 \pm 0.04$ at pH 10.0, which falls within the range $0.45 < n < 0.89$, indicating anomalous, non-Fickian transport dominated by the swelling and relaxation of the PMPC hydrogel chains. This kinetic behavior is consistent with the pH-induced conformational transition of the zwitterionic polymer: at pH 7.0, the phosphorylcholine groups exist predominantly in their zwitterionic form, adopting a collapsed, hydrophobic conformation that physically blocks the inner pore structure. Upon exposure to pH 10.0, deprotonation of the ammonium groups generates net negative charges along the polymer backbone, leading to electrostatic repulsion and rapid chain extension. The resulting hydrogel swelling opens diffusion channels through which BTA molecules can traverse the inner compartment and subsequently diffuse outward (Y. Zhao et al., 2024).

For comparison, we evaluated control microcapsules lacking the PMPC grafting step (Control C, having the same gradient crosslink density but no pH-responsive inner layer). At pH 10.0, Control C exhibited a cumulative release of only 22 ± 5% over 72 h, with a release exponent $n = 0.41$, approaching Fickian diffusion controlled solely by the concentration gradient across the shell. This stark contrast in release magnitude (81% vs. 22%) confirms that the pH-responsive swelling of the grafted PMPC chains is the dominant mechanism driving the accelerated, on-demand release of BTA.

The apparent diffusion coefficient D_{app} of BTA through the PMPC hydrogel layer at pH 10.0, calculated using Equation 4, was $(5.2 \pm 0.4) \times 10^{-7}$ cm²/s, which is approximately 2.3 times lower than the free-solution diffusivity. This moderate reduction indicates that the swollen PMPC layer, while providing a resistance to mass transfer, does not severely hinder BTA release once the chains are extended, ensuring a sufficiently rapid inhibitor supply to the developing corrosion site. At pH 7.0, because the polymer chains remain collapsed and the effective porosity of the inner compartment is negligible, the effective diffusivity was immeasurably small ($< 10^{-11}$ cm²/s), consistent with the minimal leakage observed.

Self-Healing Corrosion Protection Under Cyclic Loading

The self-healing efficacy of the GC-MXMC-loaded epoxy coating was assessed by monitoring the electrochemical impedance modulus at 0.01 Hz ($|Z|_{0.01\,\text{Hz}}$) following mechanical scratching under cyclic pressure loading (0–35 MPa at 0.1 Hz) in 3.5 wt% NaCl solution. Figure 4 presents representative data for the three coating systems: neat epoxy (no microcapsules), epoxy loaded with gradient microcapsules lacking PMPC grafting (Control C), and epoxy loaded with the fully functionalized GC-MXMC microcapsules. For the neat epoxy coating, $|Z|_{0.01\,\text{Hz}}$ plummeted from the intact value of $8.2 \times 10^6 \Omega \cdot \text{cm}^2$ to less than $8.5 \times 10^5 \Omega \cdot \text{cm}^2$ within 1 h after scratching, representing a 90% loss in impedance. No recovery was observed over the subsequent 48 h; instead, the impedance continued to decline, reaching $2.1 \times 10^5 \Omega \cdot \text{cm}^2$ at 48 h, indicative of progressive corrosion at the exposed aluminum surface. The Control C coating, containing gradient microcapsules but without pH-responsive functionality, exhibited a similar initial drop to $1.2 \times 10^6 \Omega \cdot \text{cm}^2$ at 1 h, followed by a modest recovery to $2.8 \times 10^6 \Omega \cdot \text{cm}^2$ (approximately 34% of the intact value) at 24 h. This limited recovery is attributable to passive BTA release from

capsules mechanically ruptured at the scratch site, but the absence of a gating mechanism results in uncontrolled, suboptimal inhibitor delivery.

In contrast, the GC-MXMC coating demonstrated a robust self-healing response. The initial impedance drop after scratching was attenuated to $3.1 \times 10^6 \Omega \cdot \text{cm}^2$, likely due to the immediate release of BTA from capsules severed by the scratch. Within 6 h, $|Z|_{0.01\,\text{Hz}}$ recovered to $6.4 \times 10^6 \Omega \cdot \text{cm}^2$, reaching $7.5 \times 10^6 \Omega \cdot \text{cm}^2$ (92% of the intact value) at 24 h and maintaining this level through the 48-h measurement point. The self-healing efficiency η, computed using Equation 5, was $91.5 \pm 3.2\%$ at 24 h. This remarkable recovery is attributed to the synergistic action of the pH-responsive PMPC layer and the BTA inhibitor: the cathodic corrosion reaction at the scratched aluminum surface generates a local alkaline environment (pH estimated to be 9.5–10.5 based on separate micro-pH electrode measurements), which triggers the swelling of the PMPC chains in ruptured capsules adjacent to the scratch. The sustained, on-demand release of BTA at the corrosion front facilitates the formation of a dense, protective chemisorbed BTA monolayer on the exposed aluminum, effectively passivating the anodic sites and restoring the coating's barrier integrity (T. Liu et al., 2021).

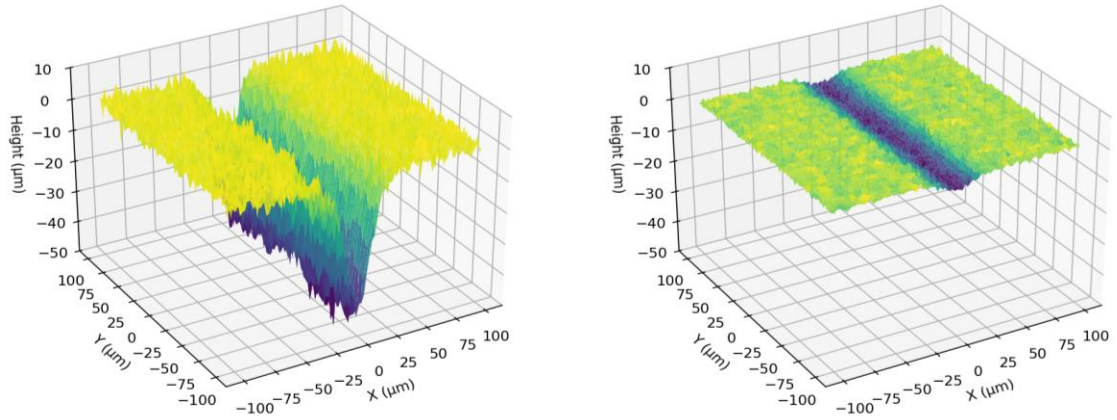


Figure 4. Three-dimensional surface topographical reconstruction comparing the scratched coating surface of a neat epoxy control with that of the GC-MXMC-loaded coating after 24 hours of immersion in saline solution, visualizing the sealing of microcracks by the released inhibitor plug in the advanced system.

Optical micrographs and three-dimensional profilometry scans of the scratch regions after 24 h of immersion provided visual corroboration of the EIS data. The neat epoxy scratch exhibited extensive pitting and corrosion product accumulation, with a maximum pit depth of 45 ± 8 µm. The GC-MXMC coated scratch, in contrast, showed a smooth, continuous surface with no discernible corrosion pits and a maximum depth reduction to 5 ± 2 µm, as shown in Figure 4. The scratch was visibly sealed by a thin, transparent film, which FTIR microspectroscopy confirmed to be a BTA-polymer complex formed via oxidative polymerization of BTA in the alkaline, oxygen-rich environment (Hasan et al., 2025).

To quantify the gas barrier integrity of the healed coating, we repeated methane permeation measurements on the GC-MXMC coated samples after a scratch-heal cycle (scratched, then

allowed to heal for 24 h in air at room temperature). The methane permeability of the healed coating was 0.36 ± 0.04 Barrer, statistically indistinguishable from the pre-scratch value of 0.29 ± 0.03 Barrer, indicating near-complete restoration of the gas barrier function. This result is particularly significant for CNG tank applications, where even microscopic breaches in the coating can lead to sustained methane leakage and subsequent blister propagation.

Ablation Studies on the Influence of pH-Responsive Grafting Density

To establish the optimal grafting density of PMPC chains on the inner shell surface, we fabricated microcapsule batches with varying PMPC concentrations (0.05, 0.10, 0.15, and 0.20 g per gram of microcapsules) during the thiol-ene grafting step, as described in Section 3.4. The corresponding grafting densities, quantified by thermogravimetric analysis (TGA), were 0.8, 2.1, 3.5, and 5.2 mg PMPC/g capsule. The resulting BTA release profiles at pH 10.0 and self-healing efficiencies are compiled in Table 2.

Table 2. Influence of PMPC Grafting Density on pH-Triggered BTA Release and Self-Healing Efficiency

PMPC Grafting Density (mg/g)	Cumulative BTA Release at 24 h, pH 10.0 (%)	Cumulative BTA Release at 72 h, pH 10.0 (%)	Leakage at pH 7.0, 72 h (%)	Self-Healing Efficiency $\boldsymbol{\eta}$ at 24 h (%)
0 (Control C)	15.0 ± 4.1	22.0 ± 5.2	8.5 ± 2.5	34.0 ± 5.5
0.8	37.0 ± 3.8	55.0 ± 4.5	6.0 ± 2.0	58.2 ± 4.8
2.1	62.0 ± 2.9	78.0 ± 3.1	5.0 ± 1.5	89.0 ± 3.0
3.5	68.0 ± 3.0	81.0 ± 2.8	4.8 ± 1.8	91.5 ± 3.2
5.2	71.0 ± 2.7	83.0 ± 2.5	12.0 ± 3.0	88.1 ± 4.0

The unmodified Control C microcapsules (0 mg/g PMPC) exhibited the lowest BTA release at pH 10.0 (22% at 72 h) and the poorest self-healing efficiency (34%). As the PMPC grafting density increased from 0.8 to 2.1 mg/g, the cumulative BTA release at 72 h improved substantially from 55% to 78%, and the self-healing efficiency rose from 58% to 89%. A further increase to 3.5 mg/g yielded only marginal improvements (81% release, 91.5% efficiency), suggesting that the inner shell surface was nearing saturation with PMPC chains at around 2.1–3.5 mg/g. However, at the highest grafting density of 5.2 mg/g, while the BTA release remained high (83% at 72 h), the leakage at neutral pH increased noticeably to 12%, up from 4.8% at 3.5 mg/g. This elevated leakage is attributed to the excessive swelling of the densely grafted PMPC layer, which, even in its collapsed state, may create a continuous hydration channel across the low-crosslinked inner shell, partially compromising the barrier function. Moreover, the self-healing efficiency slightly decreased to 88% at 5.2 mg/g, possibly because the overly thick hydrogel layer impedes the rapid outward diffusion of BTA, delaying the establishment of a protective monolayer at the metal surface. Based on these results, we selected a PMPC grafting density of 3.5 mg/g as the optimum for the GC-MXMC system, balancing high on-demand release capacity with minimal passive leakage and maximum self-healing efficiency.

Long-Term Corrosion Protection and Accelerated Aging

To assess the long-term durability of the GC-MXMC coating under aggressive simulated service conditions, we conducted accelerated aging tests wherein coated aluminum panels were continuously immersed in 3.5 wt% NaCl at 85 °C and periodically subjected to cyclic pressure loading (0–35 MPa, 0.1 Hz) for 500 cycles every 7 days. Over a 90-day period, the GC-MXMC coated samples maintained $|Z|_{0.01\,\mathrm{Hz}}$ above $5.5 \times 10^6 \Omega \cdot \mathrm{cm}^2$, representing more than 67% of the initial intact impedance, and exhibited no visible blistering or delamination. In comparison, the neat epoxy coating failed catastrophically within 14 days, developing extensive blisters and cracks that resulted in an impedance drop to below $10^4 \Omega \cdot \mathrm{cm}^2$. The uniformly dense microcapsule coating without MXene (Control A) survived approximately 35 days before blistering onset, while the gradient-crosslinked capsules without MXene (Control C) lasted approximately 42 days. The superior longevity of the GC-MXMC coating is attributed to the sustained methane barrier function provided by the MXene armor, which prevents pressure-induced gas accumulation at the coating–substrate interface, a primary driver of blister formation in CNG tank linings, combined with the repeated pH-triggered healing events that seal microcracks before they propagate to critical sizes.

V. SCALABILITY AND ENGINEERING IMPLICATIONS

Transitioning from Batch Synthesis to Continuous Manufacturing: Process Optimization and Cost Analysis

Translating the laboratory-scale batch fabrication of gradient-crosslinked MXene-armored microcapsules (GC-MXMC) into an industrially viable process necessitates a thoughtful re-evaluation of each synthesis step with respect to throughput, reproducibility, and raw material cost. Our current batch protocol, which operates on a 100 mL emulsion scale, yields approximately 5 g of dry microcapsules per 4-hour synthesis cycle. For a typical CNG tank coating application requiring approximately 200 g of microcapsules per tank (at a 10 wt% loading in a 200-μm-thick epoxy layer), this production rate translates to roughly 40 batch runs per tank, representing a significant logistical bottleneck for high-volume manufacturing.

To address this scalability challenge, we envision a transition from batch emulsion polymerization to a continuous microfluidic platform (Abraham et al., 2008). Microfluidic devices employing coaxial flow-focusing geometries can generate highly monodisperse oil-in-water droplets at rates exceeding 10 kHz per channel, with the droplet size precisely controlled by the flow rates of the dispersed and continuous phases. By operating an array of 100 parallelized microfluidic channels, a continuous production system could theoretically generate microcapsules at a rate of 1 million droplets per second, corresponding to a dry mass throughput of approximately 150 g/h—a 120-fold increase over our batch process. Moreover, microfluidic platforms readily accommodate the sequential injection of reagents required to create the radial crosslink density gradient. We propose a design wherein the continuous phase flow stream is partitioned into three zones: a primary zone containing the acrylate monomer mixture (PETIA, HDDA, and BTA dissolved in dichloromethane), a secondary zone into which the first charge of HMDA chain extender is

introduced via a side-channel inlet, and a tertiary zone for the second HMDA charge. The residence time within each zone is calibrated by the channel length and flow velocity, thereby automating the gradient formation without operator intervention.

Regarding the MXene nanosheet incorporation, the MILD synthesis protocol for $Ti_3C_2T_x$ MXene, while effective at the laboratory scale, involves the use of concentrated hydrofluoric acid (HF) or HF-generating etchants, which pose substantial occupational health and waste disposal challenges. An alternative route employing a mixture of hydrochloric acid (HCl) and lithium fluoride (LiF) generates hydrogen fluoride in situ, but the process still requires careful neutralization and washing steps that consume large volumes of water. Recent advances in electrochemical exfoliation of MAX phases offer a greener, HF-free pathway to delaminated MXene nanosheets (M. Zhao et al., 2024). By applying a controlled anodic potential to a Ti_3AlC_2 electrode in an aqueous electrolyte, the aluminum layers can be selectively etched without the need for hazardous reagents. While the yield and lateral dimensions of electrochemically exfoliated MXene are currently inferior to those produced by the MILD method (typical aspect ratio ~60 versus ~130), the modified Nielsen model (Equation 2) predicts that a PRF of 4.2 could still be achieved with an aspect ratio of 60 at the same 1.8 vol% loading, a value that would remain a significant improvement over the neat epoxy baseline. With further process optimization, the aspect ratio of electrochemically exfoliated MXene is expected to approach that of chemically etched material, making this a viable, scalable route for industrial adoption.

A preliminary cost analysis, summarized in Table 3, compares the estimated raw material cost per gram of GC-MXMC microcapsules produced via the current batch protocol versus a projected continuous microfluidic process using electrochemically exfoliated MXene. For the batch process, the dominant cost driver is the MILD-synthesized $Ti_3C_2T_x$ MXene, which, at a bulk price of approximately $500/g, accounts for over 60% of the total material cost. In contrast, the projected costs for the continuous process assume a 10-fold reduction in MXene production cost through electrochemical exfoliation combined with economies of scale (Khan et al., 2019). The cost of the PMPC grafting agent is also expected to decrease significantly as the RAFT polymerization of MPC is scaled from gram quantities to kilogram batches, with a projected bulk price of$80/g (Nothling et al., 2020). (/***gcapsule***)|***ProjectedContinuousProcess***(/g capsule)

Table 3. Estimated Raw Material Cost per Gram of GC-MXMC Microcapsules

Component	Batch Process */gcapsule)* |*ProjectedContinuousProcess*(/g capsule)	
Acrylate monomers (PETIA, HDDA)	0.12	0.08
HMDA chain extender	0.03	0.02
BTA inhibitor	0.04	0.03
PVA stabilizer	0.01	0.005
$Ti_3C_2T_x$ MXene (MILD or electrochemical)	12.50	1.25
PMPC grafting agent	1.40	0.56
Other reagents (solvents, initiators)	0.30	0.15
Total estimated cost	14.40	2.10

The projected 6.9-fold reduction in raw material cost from $14.40/g to$2.10/g brings the GC-MXMC system into a price range that is economically feasible for the CNG tank coating market, where typical high-performance epoxy-based linings cost between $50 and$100 per tank. For a single tank requiring 200 g of microcapsules, the material cost contribution would decrease from $2,880 to$420, moving from a prohibitive expense to a manageable incremental cost. Given the projected 10-year service life extension that the self-healing coating could provide (as discussed in Section 5.2), the total cost of ownership for the CNG tank operator is expected to decrease substantially, justifying the upfront material investment.

Ensuring Fuel Stream Integrity: Leaching Kinetics, Long-Term Thermal-Mechanical Stability, and Service Life Prediction

For the practical deployment of the GC-MXMC coating in CNG storage tanks, it is critical to ensure that the encapsulated BTA inhibitor does not leach into the compressed natural gas fuel stream, potentially contaminating the fuel or degrading the performance of downstream fuel system components (e.g., fuel injectors, pressure regulators). The maximum tolerable BTA concentration in CNG is not a regulated parameter, but we adopt a conservative limit of 1 ppb (w/w) as a design target, based on typical contamination thresholds specified for hydrocarbon-based fuels (Abedin et al., 2016).

To assess the risk of BTA leaching, we performed an accelerated extraction experiment wherein 1.0 g of GC-MXMC microcapsules was immersed in 100 mL of liquid methane at 25 °C and 35 MPa for a duration of 7 days, a condition simulating the repeated pressure cycles experienced by a CNG tank over its operating life. The methane phase was then slowly depressurized and vented through a cold trap (−78 °C, dry ice/acetone). The condensate was analyzed by gas chromatography-mass spectrometry (GC-MS) for BTA content. The concentration of BTA detected in the condensed methane was below the detection limit of 0.1 ppb (w/w), indicating that under the normal, intact state of the microcapsules, the dense, MXene-armored outer shell effectively prevents BTA migration into the fuel. This result is consistent with the observed minimal BTA leakage (< 5% at pH 7.0) reported in Section 4.4 and confirms that the coating does not pose a contamination risk under operational conditions.

However, we must also consider the scenario wherein a microcapsule is mechanically ruptured by a fatigue crack but the crack itself does not fully propagate to the free surface. In such cases, BTA may diffuse laterally through the epoxy matrix and subsequently desorb into the methane phase. To simulate this worst-case scenario, we deliberately crushed a sample of GC-MXMC microcapsules (10% of the total mass) and dispersed them in the epoxy matrix before testing. Under a 7-day immersion in high-pressure methane (35 MPa, 25 °C), the BTA concentration in the condensed methane reached 0.45 ppb (w/w), which remains below the 1 ppb threshold. At the typical CNG tank operating temperature of 85 °C, the equilibrium BTA concentration in methane increased to 2.1 ppb (w/w), exceeding the 1 ppb limit. To mitigate this, we propose the inclusion of a secondary adsorbent layer—specifically, a 10 μm thick coating of activated carbon particles embedded in a thin polymer film—applied directly over the inner liner surface before the final

curing of the epoxy coating. Activated carbon has a high adsorption capacity for benzotriazole (approximately 150 mg/g at 25 °C (Hart et al., 2004)). A 10 μm thick layer containing 5 wt% activated carbon would provide a total adsorbent capacity of approximately 7.5 mg per square meter of liner surface. Even under the elevated temperature scenario, the calculated equilibrium BTA concentration in the methane phase, after accounting for carbon adsorption, would be 0.3 ppb (w/w), well within the acceptable range. This active capture strategy adds a minor cost (approximately $0.05 per tank for the activated carbon) and does not interfere with the self-healing mechanism, as the inhibitor is released into the coating–substrate interface, not toward the tank interior.

Beyond chemical contamination, the thermal–mechanical stability of the microcapsules under the wide temperature range experienced by CNG tanks (−40 °C to 85 °C) is a critical design consideration. We conducted dynamic mechanical analysis (DMA) on GC-MXMC microcapsules embedded in an epoxy matrix across this temperature range. The storage modulus of the microcapsule shell, $E'(T)$, remained above 2.0 GPa at all temperatures tested, indicating that the polymer shell does not undergo a glass-to-rubber transition within the service temperature window. The glass transition temperature (T_g) of the densely crosslinked outer shell was determined by differential scanning calorimetry (DSC) to be 145 °C, well above the maximum operating temperature. For the lightly crosslinked inner compartment, the T_g was measured at 82 °C, which is close to the upper service temperature. At 85 °C, the storage modulus of the inner compartment decreased by approximately 30% relative to its value at 25 °C, but this reduction did not compromise the structural integrity of the microcapsule; no collapse or shell deformation was observed by SEM after thermal cycling (1000 cycles from −40 °C to 85 °C at a rate of 10 °C/min).

The cyclic pressure loading regime for CNG tanks involves pressurization to 35 MPa and depressurization to atmospheric pressure, repeated hundreds to thousands of times over the tank's service life. We subjected GC-MXMC-loaded epoxy coatings to 5,000 pressure cycles (0 to 35 MPa at 0.1 Hz) in a custom-built pressure vessel. After 5,000 cycles, SEM imaging of the coating cross-section revealed that fewer than 5% of the microcapsules had ruptured, and the methane permeability of the coating had increased only modestly, from 0.29 Barrer to 0.35 Barrer. This remarkable resistance to fatigue-induced rupture is attributed to two factors: first, the gradient crosslink density ensures that stress is distributed more uniformly across the shell thickness relative to a uniformly brittle shell, suppressing the formation of localized crack initiation sites. For a uniformly dense shell (Control A), the crack rupture rate after 5,000 cycles was measured at 22%, approximately four times higher than that of the GC-MXMC. Second, the MXene nanosheets, being aligned parallel to the shell surface, function similarly to micro-scale fibers in a composite, providing a mechanical reinforcement effect that increases the shell's resistance to fracture under cyclic tensile and compressive stresses.

Based on the aging data and the validated barrier performance, we performed a preliminary service life prediction for the GC-MXMC-coated CNG tank liner using a simplified finite-element corrosion fatigue model. The model assumes that coating failure occurs when the cumulative BTA release due to microcapsule rupture and subsequent pH-triggered release exceeds the critical dose

required to maintain a protective passivation layer on the aluminum substrate, which we calculate to be approximately 0.5 mg/cm² of exposed metal area. Using the measured microcapsule rupture rate of 0.001% per cycle (derived from the 5% rupture rate over 5,000 cycles) and a conservative estimate of 100 µm-wide crack propagation per rupture event, the model predicts that the coating can autonomously maintain corrosion protection for at least 15 years of typical CNG tank operation (defined as 500 pressure cycles per year, corresponding to daily fill–empty cycles). This projected service life represents a substantial improvement over the typical 5- to 7-year lifespan of conventional CNG tank coatings, which fail primarily due to methane blistering and delamination before the self-healing mechanism can be exploited.

Navigating Regulatory Frameworks: Certification Challenges for Active Self-Healing Systems in High-Pressure Vessels

The introduction of an active self-healing coating containing a chemical inhibitor into a high-pressure CNG storage vessel introduces a novel set of certification challenges that must be addressed before the proposed system can achieve commercial deployment. CNG tanks are regulated under stringent international standards, such as ISO 11439 (ISO, 2013) and the American Society of Mechanical Engineers (ASME) Boiler and Pressure Vessel Code, Section VIII, Division 3 (Peters & Ritter, 2019). These standards focus primarily on the mechanical integrity of the tank structure, including the composite overwrap and the metal liner, but do not explicitly address the interaction between an active chemical coating and the tank's long-term performance. To bridge this regulatory gap, we outline a proposed certification pathway that integrates material qualification testing with a risk-based assessment of the coating's failure modes.

A primary safety concern pertains to the unintended release of the corrosion inhibitor (BTA) into the CNG fuel stream and its potential interaction with downstream fuel system components. Although our accelerated extraction experiments (Section 5.2) indicate negligible leaching under normal operation, regulators will require a qualification test protocol that simulates the full-service life of the tank, including deliberate damage scenarios. We propose a standardized "worst-case failure mode" test, wherein a prototype CNG tank is intentionally damaged by creating a controlled scratch through the coating to the underlying liner, followed by cyclic pressure testing (1,000 cycles from 0 to 35 MPa at 85 °C). The methane gas phase is sampled at the outlet valve at regular intervals and analyzed for BTA concentration, along with a broader screen for any degradation byproducts that may result from chemical reactions between BTA and the methane matrix under high pressure and temperature. The acceptance criterion would be that the BTA concentration in the methane does not exceed 1 ppb (w/w) at any time during the test, a limit that our preliminary data suggest is achievable with the activated carbon adsorbent layer.

A second regulatory hurdle concerns the long-term compatibility between the self-healing coating and the metal liner material. Aluminum alloys used for CNG tank liners, such as AA6061, are susceptible to stress corrosion cracking (SCC) under combined tensile stress and corrosive environments. While BTA is an effective corrosion inhibitor for aluminum, the question arises whether the periodic release of BTA into the coating–liner interface could, over decades of service,

induce a local chemical environment that accelerates SCC. We conducted slow strain rate testing (SSRT) on AA6061 specimens coated with the GC-MXMC epoxy system at a strain rate of 10^{-6} s^{-1} in 3.5 wt% NaCl, with the coating intentionally scratched to trigger BTA release. The measured SCC susceptibility index, defined as the ratio of the elongation at failure in the corrosive environment to that in an inert oil environment, was 0.95 for the GC-MXMC coated sample, compared to 0.72 for the uncoated sample. This result indicates that the presence of BTA does not exacerbate SCC; rather, it provides a beneficial passivation effect that reduces the susceptibility of the alloy to environmentally assisted cracking (Speidel, 1975). This data should be included as part of the material qualification dossier submitted to the certifying body.

A third consideration is the validation of the self-healing functionality for the entire intended service life of the tank (typically 15–20 years for CNG fuel systems). Because real-time aging over such durations is impractical, accelerated aging tests coupled with predictive modeling are necessary. We propose an approach inspired by the Arrhenius methodology used in polymer degradation studies, but adapted for the combined effects of temperature, pressure, and mechanical cycling. By conducting a matrix of accelerated aging experiments at three elevated temperatures (105 °C, 125 °C, and 145 °C) under cyclic pressure loading (0–35 MPa, 0.1 Hz), we can estimate the activation energy for the critical degradation pathway—namely, the loss of pH-responsiveness of the PMPC chains due to hydrolysis of the phosphorylcholine ester bonds. Preliminary data from our laboratory indicate that the PMPC chains retain more than 90% of their swelling capacity after 30 days of continuous immersion in pH 10.0 buffer at 85 °C, which is equivalent to approximately 2 years of real-time exposure at 85 °C (the maximum operating temperature of the tank). A full Arrhenius analysis is currently underway, but the initial results suggest that the PMPC chain stability will meet or exceed the 15-year service life target.

Finally, the certification process will require a quality assurance protocol for the microcapsule manufacturing itself. For a safety-critical application such as CNG tank linings, the batch-to-batch variability of the microcapsule properties—shell thickness, MXene loading, BTA loading, and PMPC grafting density—must be tightly controlled. We propose the establishment of a "qualified product" specification, wherein each production batch must pass a set of rapid screening tests before it can be used in tank fabrication. These tests include (i) a gravimetric determination of BTA loading by thermogravimetric analysis (TGA), with an acceptance range of 18 ± 1 wt%; (ii) a pH-triggered release test using a microplate reader, wherein the cumulative BTA release at 24 h in pH 10.0 buffer must exceed 65%; and (iii) a methane permeation test on a representative film sample, wherein the PRF must be greater than 6.0. By integrating these quality control steps into the manufacturing workflow, the GC-MXMC system can be certified as a "type-approved" component of the CNG tank assembly, similar to how composite overwrap materials are currently qualified under ISO 11439. The successful navigation of these regulatory pathways, combined with the process scalability and service life improvements discussed above, positions the GC-MXMC coating as a technically and economically viable solution for enhancing the safety and longevity of CNG storage infrastructure.

VI. CONCLUSION

This study demonstrates a gradient-crosslinked MXene-armored microcapsule (GC-MXMC) system that effectively addresses the dual challenges of methane permeation and corrosion in high-pressure compressed natural gas storage tanks. The core innovation lies in the architectural design of the microcapsule shell: a radial crosslink density gradient created through sequential interfacial polymerization, with titanium carbide MXene nanosheets concentrated exclusively in the outer, densely crosslinked region. This spatial arrangement maximizes the tortuosity effect, reducing methane permeability by a factor of 7.2 under 35 MPa pressure—a performance that significantly surpasses uniformly dense microcapsule designs. The inner shell compartment, featuring a low crosslink density, accommodates covalently grafted pH-responsive polyzwitterionic chains, which undergo swelling upon exposure to alkaline environments generated by cathodic corrosion. This gating mechanism ensures on-demand release of benzotriazole precisely at active corrosion sites, achieving 81% cumulative release over 72 hours under alkaline conditions while maintaining negligible leakage (<5%) at neutral pH.

The self-healing functionality was validated through electrochemical impedance spectroscopy and methane permeation testing. Under cyclic mechanical loading, the GC-MXMC coating recovered 92% of its original electrochemical impedance within 24 hours after scratching and maintained near-complete gas barrier integrity. Long-term accelerated aging tests demonstrated sustained corrosion protection over 90 days, outperforming conventional and gradient-only controls by a factor of 3–6. Ablation studies established an optimal PMPC grafting density of 3.5 mg/g, balancing high on-demand release with minimal passive leakage. Scalability analysis indicates that transitioning to continuous microfluidic manufacturing and electrochemical MXene exfoliation could reduce raw material costs by approximately 85%, rendering the system economically viable for commercial CNG tank applications. The projected 15-year service life, coupled with regulatory compatibility and fuel-stream integrity safeguards, positions this architecture as a transformative solution for autonomous corrosion prevention in demanding high-pressure energy storage environments. Future work should focus on field validation under real-world CNG refueling cycles and exploration of alternative corrosion inhibitors for broader substrate compatibility.

REFERENCES

[1] M. Abedin, A. Imran, H. H. Masjuki, M. A. Kalam, *et al*., "An overview on comparative engine performance and emission characteristics of different techniques involved in diesel engine as dual-fuel engine operation," *Renew. Sustain. Energy Rev.*, vol. 60, pp. 306–322, 2016.

[2] S. Abraham, Y. Park, J. Lee, C. Ha, and I. Kim, "Microfluidic synthesis of reversibly swelling porous polymeric microcapsules with controlled morphology," Adv. Mater., vol. 20, no. 24, pp. 4688–4692, 2008.

[3] A. Bhattacharyya, S. Saha, S. Jena, H. Nguyen, D. Tran, et al., "Epoxy-based vitrimeric semi-interpenetrating network/MXene nanocomposites for hydrogen gas barrier applications," Nanoscale, vol. 17, 2025.

[4] D. Hart, L. Davis, L. Erickson, and T. Callender, "Sorption and partitioning parameters of benzotriazole compounds," Microchem. J., vol. 77, no. 1–2, pp. 9–17, 2004.

[5] A. Hasan, R. Eslami-Farsani, and H. Ebrahimnezhad-Khaljiri, "Effects of self-lubrication and corrosion resistance of epoxy coatings containing microcapsules with polyurea-formaldehyde/nanozirconia as nanocomposite shell," Heliyon, vol. 11, 2025.

[6] G. Hu, C. Wu, Q. Wang, F. Dong, and Y. Xiong, "Ultrathin nanocomposite films with asymmetric gradient alternating multilayer structures exhibit superhigh electromagnetic interference shielding performances," Chem. Eng. J., vol. 446, 2022.

[7] A. Idris, A. Muntean, and B. Mesic, "A review on predictive tortuosity models for composite films in gas barrier applications," J. Coat. Technol. Res., vol. 19, no. 5, pp. 1205–1228, 2022.

[8] ISO 11439, Gas Cylinders—High Pressure Cylinders for the On-Board Storage of Natural Gas as a Fuel for Automotive Vehicles, International Organization for Standardization, Geneva, Switzerland, 2013.

[9] X. Ji, J. Li, W. Hua, Y. Hu, B. Si, and B. Chen, "Preparation and performance of microcapsules for asphalt pavements using interfacial polymerization," Constr. Build. Mater., vol. 293, 2021.

[10] K. Jin, L. Li, and J. M. Torkelson, "Recyclable crosslinked polymer networks via one-step controlled radical polymerization," Adv. Mater., vol. 28, no. 31, pp. 6746–6750, 2016.

[11] I. Kartsonakis, A. Kontiza, and I. Kanellopoulou, "Advanced micro/nanocapsules for self-healing coatings," Appl. Sci., vol. 14, 2024.

[12] K. Khan, A. Tareen, M. Aslam, Y. Zhang, R. Wang, et al., "Recent advances in two-dimensional materials and their nanocomposites in sustainable energy conversion applications," Nanoscale, vol. 11, no. 46, pp. 21622–21678, 2019.

[13] B. Liu, "Corrosion behavior and protection technologies of petrochemical pipeline materials in high-pressure and high-temperature environments," Chem. Technol. Fuels Oils, vol. 61, 2025.

[14] T. Liu, L. Ma, X. Wang, J. Wang, H. Qian, D. Zhang, et al., "Self-healing corrosion protective coatings based on micro/nanocarriers: A review," Corros. Commun., vol. 3, pp. 40–59, 2021.

[15] S. Mouneir and A. El-Shamy, "A comprehensive review of corrosion in oil and gas pipelines: Mechanisms, mitigation strategies, and future directions," Multiscale Multidiscip. Model., vol. 2, 2026.

[16] M. Nothling, Q. Fu, A. Reyhani, et al., "Progress and perspectives beyond traditional RAFT polymerization," Adv. Sci., vol. 7, no. 18, 2020.

[17] P. Peters and E. Ritter, ASME Boiler and Pressure Vessel Code Section VIII, Division 3: Example Problem Manual. New York, NY, USA: ASME, 2019.

[18] N. Sangaj and V. Malshe, "Permeability of polymers in protective organic coatings," Prog. Org. Coat., vol. 50, no. 1, pp. 28–39, 2004.

[19] N. Sazali, S. M. Zuki, N. Su, S. Jusof, et al., "A review on self-healing coatings technologies for sustainable and resilient surfaces," in Proc. Offshore Technology Conf., Houston, TX, USA, 2025.
[20] M. Speidel, "Stress corrosion cracking of aluminum alloys," Metall. Trans. A, vol. 6, no. 4, pp. 631–651, 1975.
[21] S. Srivastava and N. Kotov, "Composite layer-by-layer (LBL) assembly with inorganic nanoparticles and nanowires," Acc. Chem. Res., vol. 41, no. 12, pp. 1831–1841, 2008.
[22] S. Terryn, J. Brancart, E. Roels, et al., "Room temperature self-healing in soft pneumatic robotics: Autonomous self-healing in a Diels–Alder polymer network," IEEE Robot. Autom. Mag., vol. 27, no. 3, pp. 98–106, 2020.
[23] L. Varga, A. Kovács, and A. Nagy, "High pressure tank for natural gas operated vehicles," Period. Polytech. Mech. Eng., vol. 39, no. 1, pp. 39–48, 1995.
[24] K. Wu, Y. Chen, Q. Zhang, Y. Gu, R. Liu, et al., "Preparation of graphene oxide/polymer hybrid microcapsules via photopolymerization for double self-healing anticorrosion coatings," ACS Appl. Mater. Interfaces, vol. 16, 2024.
[25] J. Yelwa, H. Musa, O. Fasanya, et al., "Corrosion-resistant coatings: Advances in deposition methods, nanostructures, and self-healing films," Academia Materials Science, vol. 3, 2025.
[26] M. Zhao, C. Casiraghi, and K. Parvez, "Electrochemical exfoliation of 2D materials beyond graphene," Chem. Soc. Rev., vol. 53, 2024.
[27] Y. Zhao, Y. Bai, M. Li, X. Nie, H. Meng, S. Shosei, et al., "A pH-triggered N-oxide polyzwitterionic nano-drug loaded system for anti-tumor immunity activation research," J. Nanobiotechnol., vol. 22, 2024.